Nanoscale

Accepted Manuscript

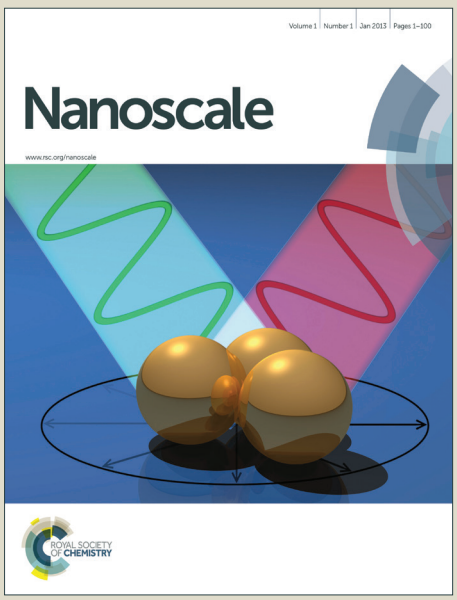

ROYAL SOCIETY OF CHEMISTRY

www.rsc.org/nanoscale

Journal Name

RSCPublishing

ARTICLE

Multifunctional $NaYF_4$:Yb, Er@mSiO_2@Fe_3O_4-PEG Nanoparticles for UCL/MR Bioimaging and Magnetically Targeted Drug Delivery

Cite this: DOI: 10.1039/x0xx00000x

Received 00th January 2012,
Accepted 00th January 2012

DOI: 10.1039/x0xx00000x

www.rsc.org/

Bei Liu [a, b], Chunxia Li, [a,*] Ping'an Ma [a], Yinyin Chen [a, b], Yuanxin Zhang [a], Zhiyao Hou [a], Shanshan Huang [a] and Jun Lin [a,*]

A low toxic multifunctional nanoplatform integrating both mutimodal diagnosis methods and antitumor therapy is highly desirable for assuring the antitumor efficiency. In this work, we show a convenient and adjustable synthesis of multifunctional nanoparticles $NaYF_4$:Yb, Er@mSiO_2@Fe_3O_4-PEG (MFNPs) based on different sizes of upconversion nanoparticles (UCNPs). With strong up-conversion fluorescence offered by UCNPs, superparamagnetism properties attributed to Fe_3O_4 nanoparticles and porous structure come from the mesoporous SiO_2 shell, the as-obtained MFNPs can not only be utilized as a contrast agent for dual modal upconversion luminescence (UCL)/magnetic resonance (MR) bio-imaging, but also achieve an effective magnetically targeted antitumor chemo-therapy both *in vitro* and *in vivo*. Furthermore, the UCL intensity UCNPs and the magnetic properties of Fe_3O_4 in the MFNPs were carefully balanced. Silica coating and further PEG modifying can improve the hydrophilicity and biocompatibility of the as-synthesized MFNPs, which were testified by the *in vitro*/*in vivo* biocompatibility and *in vivo* long-time bio-distributions. Those results revealed that the UCNPs based magnetically targeted drug carrier system we synthesized here has great promise in the future multimodal bio-imaging and targeted therapy of cancer.

1. Introduction

In the past few years, Ln^{3+}-doped upconversion nanoparticles (UCNPs) as a rising new star have provoked more and more attention in biomedical fields, which originate from their captivating merits such as high chemical stability, low auto-fluorescence, high signal-to-noise ratio, detection sensitivity, penetration depth and good biocompatibility.[1-9] In particular, spurred by the great progress in the controlled synthesis of uniform UCNPs and followed surface modification, UCNPs-based nanocomposites that combine with other functional nanoparticles such as super-paramagnetic Fe_3O_4,[10-13] ultrasmall Au[14-15] and CuS[16] in one hybrid system can act as multifunctional "theranostic" platforms and provide new possibility for the synergistic diagnosis and therapy of disease. Among various nanomaterials, the nanocomposites combining with upconversion luminescence and magnetic properties as well as porous structures are a class of novel carriers for drug delivery and multimodal bioimagings.[17] On the one hand, such nanomaterials can offer dual modal bioimagings including upconversion luminescence (UCL) imaging and magnetic resonance imaging (MRI), which may simultaneously achieve high spatial resolution and penetration depth for clinical diagnosis.[18-24] On the other hand, the composite nanoparticles containing super-paramagnetic Fe_3O_4 are a class of promising magnetic targeted "smart" drug delivery system, which is one of effective route to ameliorate the major hurdles in current chemotherapy such as the low accumulation concentration of therapeutic drugs at targeted location, the toxic side effects of drugs to the healthy cells and tissues as well as unspecific uptake of normal cells.[25-28] As such, it is of great importance to integrate UCNPs with Fe_3O_4 and porous structure to enhance the tumor-targeted drug delivery with elevated local dosages and multimodal bioimagings.

Porous SiO_2 is considered as one of the most promising porous structures for drug delivery applications, as it generally possesses good bio-compatibility and ease of surface functionalization that provides reservoirs for loading various antitumor drug molecules and active sites for linking other biological or targeted molecules by covalent association.[29-31] Therefore, taking use of mesoporous silica as intermediate layer to combine UCNPs with Fe_3O_4 can help us establish UCNPs-based magnetically targeted drug delivery systems. Furthermore, the intermediate mesoporous silica shell could not only solve the problems of lattice mismatch and chemical dissimilarity between those two kinds of nanoparticles, but also somehow protect UCNPs from the luminescence quenching by Fe_3O_4.

To our knowledge, previous studies that combined Fe_3O_4, mesoporous silica with UCNPs by two-step sol-gel process[11, 32-

[34] involved multistep and complicated procedures. In addition, the UCNPs were deposited on the surface of Fe_3O_4 or mesoporous silica by calcination, which would lead to the inreversible particle aggregations and uneven size distribution. In order to address these problems, here we design a more facile methodology to synthesize hybrid nanostructure $NaYF_4$:Yb, Er@mSiO_2@Fe_3O_4-PEG (MFNPs) that can simultaneously combine UCL, MRI and magnetically targeted drug delivery in one system. UCNPs with different sizes were directly encapsulated with the mesoporous silica through a phase-transfer-assisted surfactant-templating coating process. Then ultrasmall Fe_3O_4 nanocrystals were decorated onto the surface of mesoporous silica shell by nucleophilic substitution reaction. In order to achieve the enough bright upconversion luminescence intenisty while maintain the magnetic performance of Fe_3O_4, optimal reaction conditions were conducted carefully by changing the size of UCNPs and the amounts of Fe_3O_4 immobilized on the surface of UCNPs@mSiO_2. The capacity of loading anticancer drug doxorubicin (DOX), *in vitro* and *in vivo* biocompatibility, *in vivo* magnetically targeted tumor therapy efficacy and biodistribution as well as *in vitro* UCL and MR imaging of the as-synthesized MFNPs were also investigated in detail.

2. Experimental

2.1 Materials

All the chemical reagents were directly used without further purification. The rare earth oxides Y_2O_3, Yb_2O_3 and Er_2O_3 (99.999 %) were purchased from Science and Technology Parent Company of Changchun Institute of Applied Chemistry. Sodium fluoride (NaF), Oleic acid (OA), Cetyltrimethylammonium bromide (CTAB), Tetraethylorthosilicate (TEOS), Ammonium nitrate (NH_4NO_3), Sodium hydroxide (NaOH), Ammonium fluoride (NH_4F), Ammonium hydroxide (NH_3•H_2O), Citrate acid ($C_6H_8O_7$), n-hexane and Cyclohexane were all purchased from Beijing Chemical Reagent Company. Octadecene (ODE), 3-Aminopropyltriethoxysilane (APTES), 2-Bromo-2-methyl-propionic acid (BMPA) and Ferric acetylacetonate ($Fe(acac)_3$) were purchased from Aldrich. PEG succinimidyl carbonate (PEG-SC) was purchased from Beijing Kaizheng Bio-technology Company (China). Doxorubicin hydrochloride (DOX) was purchased from Nanjing Duodian Chemical Limited Company (China). The YCl_3, $YbCl_3$, and $ErCl_3$ solutions were prepared by dissolving the corresponding rare-earth oxides in hydrochloric acid aqueous solution followed by removal of the hydrochloric acid through evaporation.

2.2 Synthesis of $NaYF_4$:Yb, Er (UCNPs) and Fe_3O_4 Nanocrystals

Three different sizes of $NaYF_4$: 20% Yb, 2% Er nanoparticles were fabricated according to the method reported previously[35] with a little modification of the reaction solvents, temperature and time (20 nm core: 6 mL OA/15 mL ODE at 300 ^oC for 1 h; 33 nm core: 6 mL OA/15 mL ODE at 320 ^oC for 2 h; 55 nm core: 3 mL OA/17 mL ODE at 320 ^oC for 2 h). Oleic acid (OA) modified Fe_3O_4 nanocrystals were successfully synthesized following a previously reported synthesis method with a little modification. [36-37] The synthesis process was described as follows: Firstly, 0.353 g of $Fe(acac)_3$, 1.5 mL of OA, 1.5 mL of OM and 10 mL of benzyl alcohol were mixed totally before transferred into a Teflon bottle (50 mL), sealed and maintained at 180 ^oC for 10 h. As the autoclave cooled naturally, excess ethanol was added and isolated by centrifugation. Then the surfactants OA molecules modified on the surface of Fe_3O_4 nanocrystals were replaced by BMPA in order to attach Fe_3O_4 nanocrystals on the surface of mesoporous silica. The reaction for ligand exchange is as follows: a mixture of Fe_3O_4 nanocrystals (about 15 mg), BMPA (0.5 g) and citrate acid (0.05 g) was dispersed in 16 mL of chloroform/DMF (v/v=1:1) solution and kept stirring overnight at 30 ^oC.[38] The resulted BMPA-capped Fe_3O_4 nanocrystals were obtained by centrifugation and redispersed in 10 mL ethanol for further use.

2.3 Synthesis of UCNPs@mSiO_2@Fe_3O_4-PEG Nano-composites

In a typical synthesis for UCNPs@mSiO_2@Fe_3O_4-PEG (MFNPs), first of all, the UCNPs@mSiO_2 nanoparticles were obtained as follows: the oleic acid capped UCNPs (22nm, about 20 mg) and CTAB (0.1 g) were mixed in 30 mL distilled water to form a transparent solution through stirring before the addition of 150 μL of NaOH solution (2 M) and 200 μL of TEOS. UCNPs@SiO_2 was formed after the as-obtained mixture was maintained at 70 ^oC for 1 h under vigorous magnetic stirring. The pore-generating template CTAB was further removed by refluxing the above UCNPs@SiO_2 in the NH_4NO_3 ethanol solution at 60 ^oC for 2 h. Then 200 μL of APTES was added into 20 mL of UCNPs@mSiO_2 ethanol solution under stirring overnight in order to functionalize UCNPs@mSiO_2 nanospheres with amine groups.[39] Thirdly, in order to obtain UCNPs@mSiO_2@ Fe_3O_4 nanocomposties, the BMPA-capped Fe_3O_4 nanocrystals were mixed with 15 mL of the amine-functionalized UCNPs@mSiO_2 ethanol solution under magnetic stirring overnight. After centrifugation, the UCNPs@mSiO_2@Fe_3O_4 nanoparticles were obtained. Finally, PEG-stabilized UCNPs@mSiO_2@Fe_3O_4 (MFNPs) were prepared by mixing the as-obtained UCNPs@mSiO_2@Fe_3O_4 with PEG-SC (20 mg) overnight to induce covalent bonding between residual amine groups of UCNPs@mSiO_2 and PEG-SC. After removal of unreacted PEG-SC by centrifugation, the resulting MFNPs were dispersed in water.

2.4 *In Vitro* Magnetic Resonance Imaging

In vitro MR imaging experiment of MFNPs was performed in a 0.5 T MRI magnet (Shanghai Niumai Corporation Ration NM120-Analyst). MFNPs with different Fe concentrations (determined by Inductively Coupled Plasma Atomic Emission Spectrometer (ICP-AES)) were dispersed in water for the tests. The obtained relaxation time T_2 values were recorded and plotted as $1/T_2$ versus molar concentration of Fe (mM).

2.5 *In Vitro* Cytotoxicity of the MFNPs Nanocomposites

A typical MTT [3-(4,5-dimethylthiazol-2-yl)-2,5-diphenyltetrazolium bromide] cell assay was carried out to investigate the *in vitro* cytotoxicity of MFNPs. Briefly, HeLa cells were planted out in a 96-well plate (6000 cells per well) and incubated in 5% CO_2 at 37 ^oC overnight. After the cells attached to the wells, MFNPs solutions with concentrations of 1.9, 3.9, 7.8, 15.6, 31.2, 62.5, 125, 250, 500 μg/mL respectively, were added into wells and incubated for another 24 h. Then MTT solution (20 μL, 5

mg/mL) was added to each well and further incubated in 5% CO2 at 37 °C for 4 h. After that, 150 μL of DMSO were added to each well after carefully removing the original culture medium. The absorbance of the suspension was recorded by a microplate reader at the wavelength of 490 nm.

2.6 *In Vitro* Drug Storage and Release

In vitro drug storage of MFNPs was carried out by mixing the MFNPs (about 10 mg) with 2 mL DOX solution (1 mg/mL) under magnetic stirring overnight at 37 °C. The obtained DOX loaded MFNPs were collected by centrifugation and denoted as MFNPs-DOX. The amount of the DOX that loaded into the MFNPs was determined by UV-Vis spectral measurement. Then the as-obtained MFNPs-DOX were dispersed in 2 mL of pH = 7.0 and 5.0 phosphoric acidic buffer solutions (PBS) at 37 °C under magnetic stirring, respectively. At predetermined time intervals, 2 mL of fresh PBS was replaced for the original PBS in order to determine the amount of the released DOX by UV-Vis spectral measurement.

2.7 *In Vitro* Cytotoxicity of the DOX Loaded MFNPs

HeLa cells were seeded in a 96-well plate (6000 cells per well) and incubated (37 °C, 5% CO_2) overnight. Free DOX, MFNPs-DOX and pure MFNPs with different concentrations were added to the wells of 96-well plate respectively and the cells were further incubated for another 24 h. The concentrations of DOX were 0.78125, 1.5625, 3.125, 6.25, 12.5, and 25 μg/mL, respectively, while the corresponding concentrations of pure MFNPs were 15.63, 31.25, 62.5, 125, 250, and 500 μg/mL, respectively. The following steps were same with the previously mentioned MTT cell assay and the final fraction surviving of HeLa cells was measured by a microplate reader at the wavelength of 490 nm.

2.8 Cellular Uptake and Upconversion Luminescence Imaging of MFNPs

Cellular uptake degree of MFNPs was determined by flow cytometry method as follows: HeLa cells were seeded in 6-well culture plates (3×10^5 cells per well) and incubated (37 °C, 5% CO_2) overnight. Then the cells were treated with MFNPs-DOX for 0 min, 30 min, 2 h and 4 h respectively. After reaching the predetermined time, the cells were prepared consecutively by trypsinization, washing with PBS three times, and filtration through 35 mm nylon mesh. Finally FACSCalibur flow cytometer (BD Biosciences) was used to test the cellular uptake degree of MFNPs. The upconversion luminescence imaging of MFNPs was also carried out as follows: HeLa cells were seeded in 6-well culture plates (3×10^4 cells per well) and incubated (37 °C, 5% CO_2) overnight. MFNPs solution (2 mL, 200 μg/mL) was added into each well and incubated for 0.5 h and 4 h, respectively. After that, the cells were carefully washed with PBS three times, fixed with 2.5% formaldehyde for 10 min and washed again with PBS three times. The final UCL was watched by the up-conversion luminescence microscopy (UCLM), which was rebuilt on an inverted florescence microscope (Nikon Ti-S) and an external CW 980 nm diode laser.

2.9 *In Vivo* Biocompatibility of MFNPs

Female Kunming mice (25-35 g) were purchased from Center of Experimental Animals, Jilin University (Changchun, China), and the animal experiments agreed well with the criterions of The National Regulation of China for Care and Use of Laboratory Animals. Ten healthy mice were randomly divided into two groups, one group was treated with 0.2 mL of MFNPs (40 mg/kg) while the other was treated with 0.2 mL of saline as control. The weights of the mice were measured every two days. In order to further investigate the biocompatibility of MFNPs, after 12 days treatment, the mean organs of mice, such as liver, spleen, heart, lung, and kidney, were removed and fixed in 4% paraformaldehyde solution for histological examination. The serum of mice collected from both the treated group and control groups were also sent for the chemistry tests analysis. Briefly, about 0.8 mL of blood from each mouse was collected by quickly removing the eyeball from the socket. The serum was retrieved by centrifugation.

2.10 *In Vivo* Magnetic Targeting Effect of MFNPs

Eight healthy female Kunming mice (25-35 g) were chosen for the following test. The tumors were established by subcutaneous injection of H22 cells (murine hepatocarcinoma cell lines) in the left axilla of mice. After the tumors grew 5 days to reach the size of around 100-200 mm^3, the tumor-bearing mice were injected with MFNPs (12 mg Y^{3+}/kg) by tail vein injection. Then the treated mice were randomly divided into two groups (n = 4, each group): one group was managed to attach a -magnet at the left axilla of each mouse (right on the tumor), while the other group kept magnet away. After two hours, all the mice were sacrificed and the tumors were collected and solubilized by HNO_3 and H_2O_2 (v:v=1:2) at 70 °C for ICP-AES measurement of Y^{3+}.

2.11 *In Vivo* Targeted Antitumor Efficacy of DOX Loaded MFNPs

The 24 tumor-bearing mice were randomly divided into four groups (n = 6, each group), treated with free DOX, MFNPs-DOX without magnetic field (labeled as MFNPs-DOX), MFNPs-DOX with an external magnet right outside the tumor (labeled as MFNPs-DOX+MR) and saline as control by tail vein injection respectively. We injected the above materials by two times on day 1 and 5 and the injected DOX dose was 5.0 mg/kg body weight at each time points. The body weights and tumor volumes were monitored every two days. After 12 days, the tumors were dissected and weighed to evaluate the therapeutic efficacy. The tumor volume was calculated by: Tumor volume (V) = length×$width^2$/2. Relative tumor volume was calculated as V/V_0 (V_0 was the corresponding tumor volume before the treatment). Tumor growth inhibition rate was determined as (C-T)/C×100 (C was the average tumor weight of the control group and T is the average tumor weight of each treated group).

2.12 Biodistribution of Nanoparticles in Major Organs of Mice

The 16 healthy female Kunming mice weighted about 20-25 g were treated with MFNPs (12 mg Y^{3+}/kg) by tail vein injection

and then randomly divided into four groups (n = 4, each group), euthanized at four different time points (1 h, 12 h, 2 day, and 7 day) individually. Major organs such as heart, liver, spleen, lung and kidney were carefully collected, weighed and finally treated with HNO_3 and H_2O_2 (v:v=1:2) at 70 °C. The final solutions were sent to test the concentrations of Y^{3+} ion by ICP-AES.

3. Results and discussion

3.1 Controlled Fabrication and Characterization of MFNPs

In the present work, we detailed a simple synthetic route to produce different sizes of UCNPs-based magnetically targeted

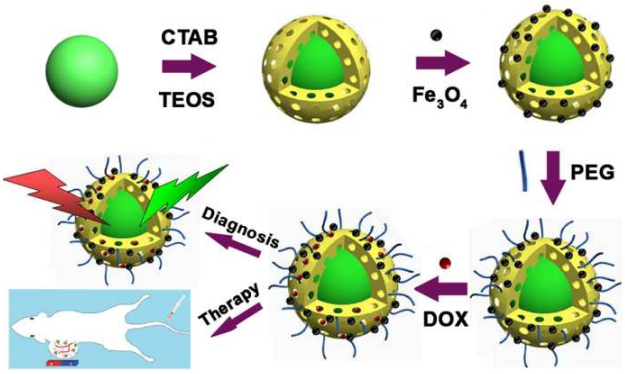

Scheme 1 Schematic illustration for the synthesis of core-shell structured $NaYF_4$:Yb, Er@$mSiO_2$@Fe_3O_4-PEG multifunctional nanoparticles (labeled as MFNPs) and subsequent bio-applications in diagnosis and anti-tumor therapy.

drug delivery carriers $NaYF_4$:Yb, Er@$mSiO_2$@Fe_3O_4-PEG (MFNPs). The overall fabrication procedure of MFNPs was illustrated in Scheme 1. Firstly, monodisperse $NaYF_4$:Yb, Er UCNPs with different sizes (20 nm, 33 nm and 55 nm) were successfully synthesized via a solvent thermal process by varying the reaction temperature, reaction time and the molar ratio of solvents OA/ODE (Figure 1a, d, g). The as-obtained UCNPs with different sizes have the similar properties, for example, they were all modified by hydrophobic OA molecules that can be well dispersed in a variety of nonpolar solvents, such as cyclohexane and trichloromethane. Under 980 nm laser excitation, as shown in Figure 1j and insets, the raising size of UCNPs from 20 nm to 55 nm would help to increase the green emission intensity centered at 521, 540, and 654 nm that ascribable to $^2H_{11/2}\rightarrow{}^4I_{15/2}$, $^4S_{3/2}\rightarrow{}^4I_{15/2}$, and $^4F_{9/2}\rightarrow{}^4I_{15/2}$ transitions of Er^{3+}, respectively, mainly because of the suppressed surface quenching,[40-41] which could be of great benefits for the further bioimaging applications. Subsequently, the as-obtained UCNPs with three different sizes were directly encapsulated with the mesoporous silica through a phase-transfer-assisted surfactant-templating coating process by applying CTAB as secondary surfactant (Figure 1b, e, h). In this process, directly coating of silica shell onto different sizes of UCNPs was achieved by adjusting the initial molar ratio of UCNPs/TEOS. Then APTES was used to provide amine

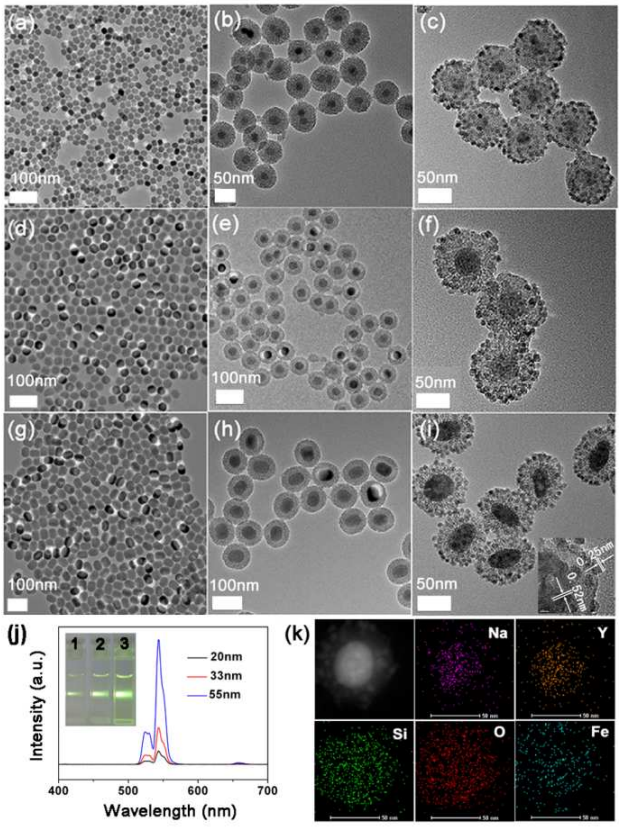

Figure 1 TEM images of $NaYF_4$: Yb, Er nanoparticles (UCNPs) with different sizes (a: 20nm, d: 33nm, g: 55nm), and their corresponding TEM images of core-shell composite nanospheres UCNPs@$mSiO_2$ (b, e, h) and UCNPs@$mSiO_2$@Fe_3O_4 (c, f, i). Inset in (i) is HRTEM image of UCNPs@$mSiO_2$@Fe_3O_4. (j) Upconversion emission spectra of UCNPs dispersed in cyclohexane (0.05 M) with different sizes under 980 nm laser excitation. Inset in (j) are the digital photographs of corresponding upconversion emission under the excitation of 980 nm laser (1: 20nm, 2: 33nm, 3: 55nm). (k) The corresponding HAADF-STEM-EDS mapping images of single UCNPs@$mSiO_2$@Fe_3O_4 nanoparticle.

functional groups on UCNPs@$mSiO_2$ nanpspheres which could serve as anchor points for further reactions. After that, the ultrasmall and multiple Fe_3O_4 nanocrystals were decorated onto the surface of mesoporous silica shell by nucleophilic substitution reaction. Figure 1c, f, i demonstrate that the UCNPs@$mSiO_2$@Fe_3O_4 based on different sizes of UCNPs retain their original morphology except for the uniform shaggy surface decoration with tiny Fe_3O_4 nanocrystals. Note that Fe_3O_4 nanocrystals decorated in the multifunctional nanoparticles could not only provide as T_2 positive agent of superparamagnetic species, but also serve for the magnetically targeted drug delivery. Finally, to make the as-synthesized nanoparticles biocompatible, PEG-SC was chosen as a hydrophilic agent to modify the nanocomposites. [42] Since all of the MFNPs based on different sizes of UCNPs were successfully fabricated and have almost the same morphology

and phase composition, we choose to take the MFNPs based on biggest size of UCNPs as an example to do the following researches because of their improving UCL intensity.

The XRD patterns of UCNPs, pure Fe_3O_4 and MFNPs were shown in Figure S1 (Supporting Information). As we can see from Figure S1a and b, the diffraction peaks of the Fe_3O_4 and UCNPs can be indexed respectively as pure cubic phase structure Fe_3O_4 (JCPDS 65-3107) and hexagonal phase structure β-$NaYF_4$ (JCPDS 16-0334). However, the obtained MFNPs (Figure S1c) were mainly ascribed to β-$NaYF_4$ structure besides an amorphous silica structure peak at $2\theta = 22°$, showing a very weak diffraction peaks of the Fe_3O_4 nanoparticles. This is perhaps because of the low concentration and subsize of Fe_3O_4 decorated in the MFNPs comparing with the UCNPs@$mSiO_2$ nanocomposites. The corresponding HRTEM image (inset of Figure 1i) can cover this insufficient section of the XRD pattern, which clearly shows the lattice fringes with interplanar spacing of 0.52 nm indexed to the (100) plane of β–$NaYF_4$ and 0.25 nm indexed to the (311) plane of Fe_3O_4. The elemental mapping images also show the uniformly distributed Na, Y, Si, O and Fe elements in single nanoparticle (Figure 1k), further confirming the successful linking of Fe_3O_4 on the UCNPs@$mSiO_2$ nanoparticles.

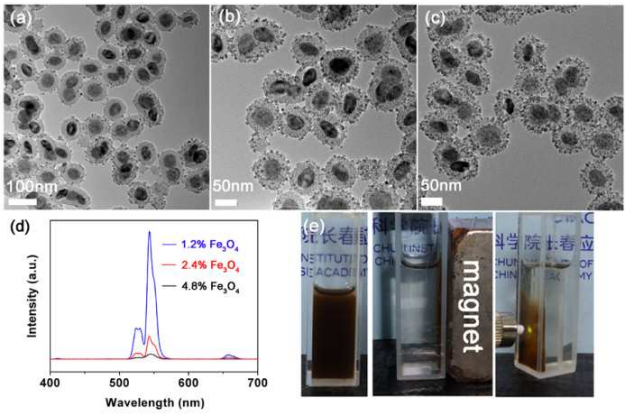

Figure 2 TEM images of UCNPs@$mSiO_2$@x wt% Fe_3O_4 with different Fe_3O_4 attached on the silica shell (a: x=1.2; b: x=2.4; c: x=4.8) and the corresponding upconversion emission spectra (d) under 980 nm laser excitation (blue line: x=1.2; red line: x=2.4; black line: x=4.8; the nanoparticles were dispersed in ethanol with a same UCNPs concentration of 20 mM). (e) Photos of MFNPs sample in an aqueous solution under ambient light (left), with a neighboring magnet (middle) and exposed to a 980 nm laser (right).

In addition, because of the nonspecific absorbency of Fe_3O_4 nanocrystals,[43] the UCL intensity of UCNPs could be significantly quenched after decorating the Fe_3O_4 nanoparticles on UCNPs@$mSiO_2$. In order to meet the various demands of magnetic and optical properties simultaneously, we take a serious of experiments to adjust the amount of Fe_3O_4 nanoparticles in MFNPs. By decreasing the dosage of Fe_3O_4 reactants in the system, the amount of Fe_3O_4 nanoparticles attached on the silica shell decreased obviously (Figure 2a-c) while the luminescence intensity of MFNPs with the same UCNPs concentration (20 mM) increased clearly (Figure 2d). Therefore, suitable amounts of Fe_3O_4 nanoparticles could be attached on the UCNPs@$mSiO_2$ nanoparticles to get enough bright luminescence intensity, while remain the magnetic performance of Fe_3O_4 nanocrystals in MFNPs. According to this baseline, the UCNPs@mSiO2@2.4%Fe_3O_4 nanoparticles in Figure 3b were chosen for the following experiments, which have both a proper luminescence intensity to satisfy the bioimaging applications and strong magnetic performance for magnetic targeted drug delivery (Figure 2e). In this way, the as-synthesized MFNPs could perfectly satisfy the anticipations for further bioapplications.

The N_2 adsorption/desorption isotherm in Figure S2 of the Supporting Information shows a type-IV isotherm and the corresponding pore size distributions of MFNPs nanospheres was very uniform with an average size of 2.4 nm. Moreover, it could be determined that the Brunauer–Emmet–Teller (BET) surface area of the as-obtained MFNPs was about 458 m^2/g and the total pore volume was 0.45 cm^3/g. All those results indicate that the mesoporous silica shell of MFNPs was capable of loading sufficient amount of drugs for drug delivery applications.

3.2 *In Vitro* and *in Vivo* Toxicology Studies of MFNPs

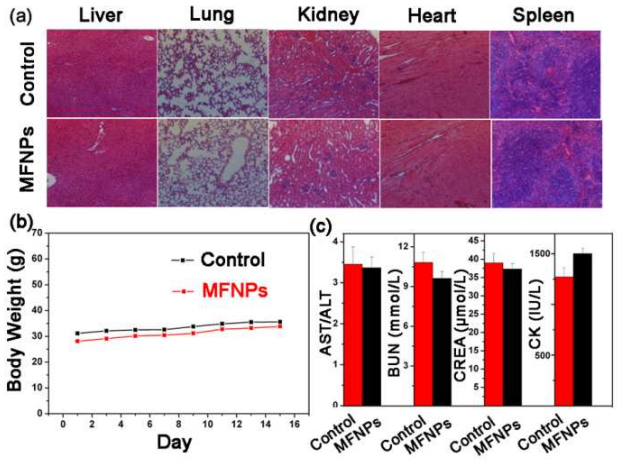

Figure 3 Systematic analysis of toxicity for MFNPs (40 mg kg^{-1}) on healthy Kunming mice. (a) Hematoxylin and eosin (H&E) stained images of major organs for control group and MFNPs group. (b) Changes in body weights of mice after two doses intravenous injection in MFNPs group and control group. (c) Blood analysis data for mice of control group and MFNPs group respectively.

In vitro/in vivo toxicology of MFNPs is a very important prerequisite for a potential anti-tumor drug carrier. Firstly, *in vitro* cytotoxicity of the MFNPs was tested by a standard MTT assay on HeLa cells. As shown in Figure S3a of the Supporting Information, HeLa cells were not impaired with a concentration of as high as 500 μg/mL after the 24 h culture. Moreover, after incubation of 24 h with MFNPs, the fluorescence microscopy images of HeLa cells were in good condition and began to

proliferate (Figure S3b, c), which means that the biocompatibility of the MFNPs could satisfy the requirements as potential drug carriers for biological applications.

In vivo toxicology studies on Kunming mice were also carried out to further make sure that the MFNPs were suitable for further bio-applications. We can conclude that all the mice treated by tail vein injection with the MFNPs (40 mg/kg) were survived in good condition from the following experimentation results: (i) The gross anatomy and pathomorphology examinations (Figure 3a) show that the main organs, including heart, liver, spleen, lung and kidney were healthy with no obvious sign of organ damage from both the control group and MFNPs group; (ii) The body weights of mice in MFNPs group increased normally without any differences with the control group (Figure 3b); (iii) The biochemical and hematological analyses of blood on the treated mice show that all the tested biochemical parameters, including aspartate aminotransferase (AST)/alanine aminotransferase (ALT), creatine kinase (CK), blood urea nitrogen (BUN) and creatinine, were in the normal range without any dysfunctions (Figure 3c). From all the above results, we could conclude that the MFNPs have a negligible side effect for further *in vivo* biomedical applications and could act as a biocompatible drug delivery to restrain tumors.

3.3 DOX encapsulated in MFNPs for chemotherapy

To be a drug delivery carrier, the drug loading and controlled release ability of MFNPs should be carefully studied.[44] Firstly,

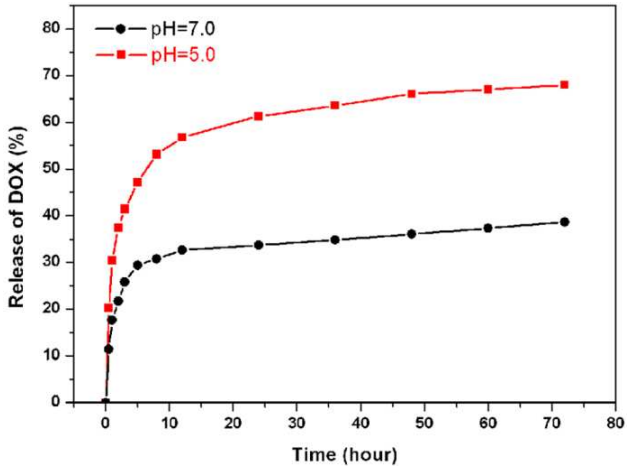

Figure 4 Cumulative DOX release from MFNPs nanocomposite spheres at pH=7.0 (black line) and pH=5.0 (red line) PBS buffer.

the antitumor chemotherapeutic drug-doxorubicin (DOX) was chosen to be loaded into the mesoporous SiO_2 of MFNPs as the model drug. The drug release percentage from DOX-loaded MFNPs complexes were evaluated at 37 °C in PBS solution (pH = 7.0 & 5.0). As shown in Figure 4, the *in vitro* DOX release profiles were obviously pH-depended: only 35% of DOX was released after 74 h at pH 7.0, while 68% of DOX released when pH decreased to 5.0. This tendency was ascribed to the increased hydrophilicity of DOX resulting from the promoted protonation of amino group when the pH was lower. Since the extracellular pH of solid tumors presents a much acidic microenvironment than the normal tissues,[45] this DOX release tendency was beneficial as a drug carrier for targeted tumor drug release. In this way, the as-synthesized MFNPs could be used as a potential drug carrier for pH dependent anti-tumor drug release.

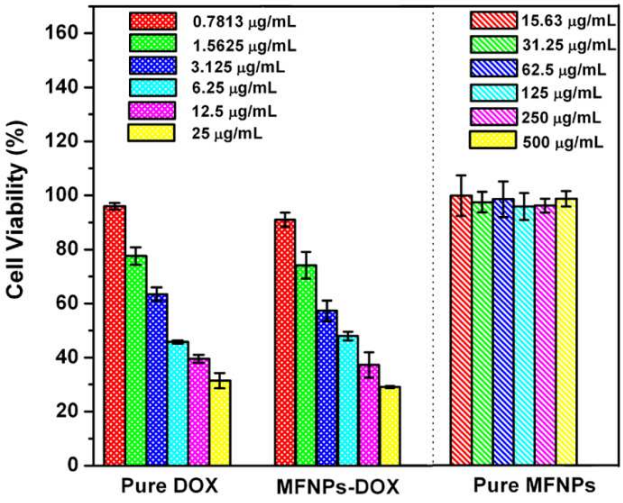

Figure 5 *In vitro* cytotoxicity of free DOX, MFNPs-DOX, and pure MFNPs against HeLa cell after 24 h incubation.

Although the loaded DOX could be released from the MFNPs in a pH dependent pattern, the *in vitro* cytotoxic effect of DOX loaded MFNPs should be further verified. Therefore, a standard MTT assay was carried out to evaluate the cytotoxic effect against HeLa cells after incubating in culture medium containing free DOX, MFNPs-DOX and pure MFNPs nanospheres for 24 h at different concentrations. As shown in Figure 5, the DOX loaded MFNPs had comparable cytotoxicity with free DOX at the same concentration of DOX, which indicated that the DOX loaded MFNPs was pharmacologically active as a potential drug carrier.

3.4 UCL/MR Imaging of MFNPs

The cell uptake process was measured by flow cytometry test. Firstly, DOX was loaded into the mesoporous SiO_2 shell of MFNPs so that the cell uptake degree can be detected by flow cytometry through the red fluorescence of DOX. As shown in Figure 6a, after incubation of HeLa cells with MFNPs-DOX fordifferent times (30 min, 2 h and 4 h), the cell uptake efficiency is increasing obviously with time progressing. Therefore, MFNPs-DOX nanospheres could be gradually taken up by HeLa cells. This effective incubation is a crucial prerequisite for the bio-applications of MFNPs. Then *in vitro* UCL imaging of MFNPs was investigated by utilizing a modified inverted fluorescence microscopy under the excitation of 980 nm laser. As presented in Figure 6b, a weak UCL signal was seen after the incubation with HeLa cells for 30 min. As the prolonging of time, stronger UCL signal could be seen,

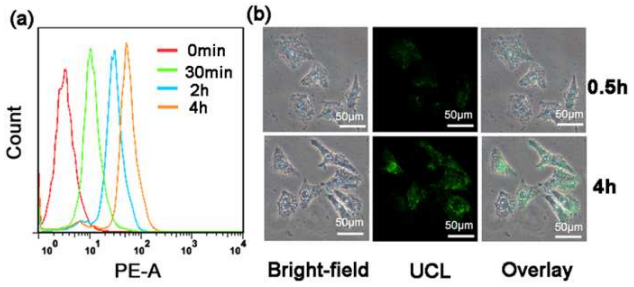

Figure 6 (a) Flow cytometry analysis of HeLa cells incubated with MFNPs-DOX for 0 min, 30 min, 2 h and 4 h. (b) Inverted florescence microscope images of HeLa cells incubated with MFNPs for 0.5 h and 4 h at 37 °C. Each series can be classified to the bright-field image, upconversion luminescent image (UCL) and the overlay of the above, respectively.

indicating that more MFNPs were incubated into the HeLa cells. This phenomenon suggested that the MFNPs can be taken up by human cells gradually and act as a successful UCL signal probe for cell imaging.

Since the ultrasmall Fe_3O_4 nanocrystals were decorated onto the surface of UCNPs@mSiO_2 by nucleophilic substitution reaction, the as-synthesized nanocomposites show

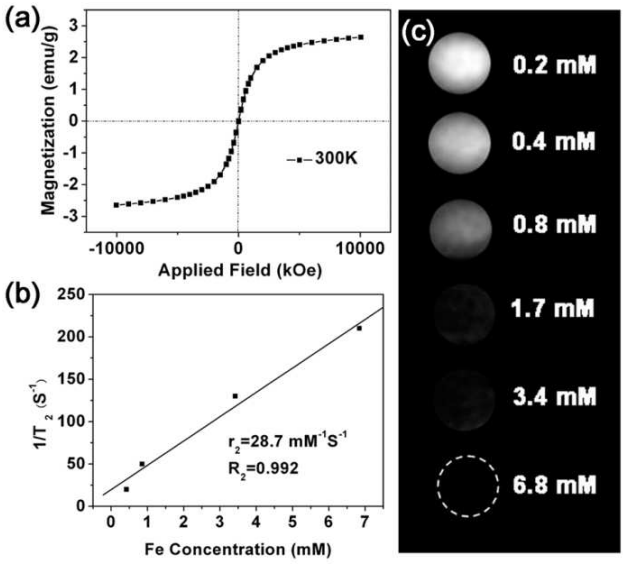

Figure 7 (a) The magnetization as a function of applied field for the as-synthesized MFNPs at 300 K. (b) Relaxation rate R2 ($1/T_2$) versus different mass concentrations of MFNPs at room temperature. (c) T_2-weighted MR images of MFNPs at different [Fe] concentrations.

superparamagnetism properties, as revealed by field-dependent magnetization measurement (Figure 7a). A low magnetic saturation is also shown in Figure 7a, perhaps due to the decreased interparticle interactions and low amount of Fe_3O_4 particles on the silica shell. T_2-weighted MR images of MFNPs revealed a concentration-dependent darkening effect (Figure 7c), with a transverse relaxivity (r_2) of 28.7 mM^{-1} S^{-1} (Figure 7b) through a linear regression curve fitting of inverse relaxation times plotted against the Fe ion concentration. The above results reveal that the MFNPs could act as a useful T_2 contrast agent for T_2-weighted MR imaging. In this way, the obtained MFNPs can offer UCL/MR dual modal bioimagings, which could simultaneously achieve high spatial resolution and penetration depth for clinical diagnosis.[46]

3.5 *In Vivo* Magnetic Targeting Effect of MFNPs

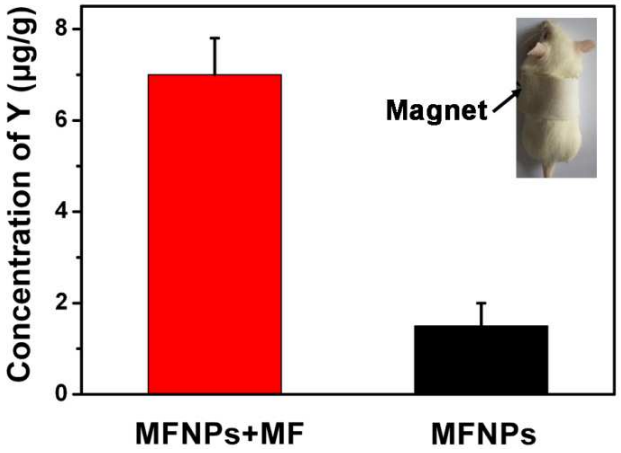

Figure 8 Magnetically targeted accumulation of MFNPs in mice determined by ICP-AES measurement of Fe concentrations (2 h post injection) and photographs (inset) of mouse treated with magnetic tumor targeting.

The targetability of a fantastic theranostic probe is highly desirable for assuring the anti-tumor efficiency. In order to test the magnetic targeting effect of MFNPs *in vivo*, the tumor-bearing mice injected with MFNPs (12 mg Y^{3+}/kg) with or without a magnet were sacrificed at 2 h post injection and the Y^{3+} concentrations of the tumors were shown in Figure 8. For the mice treated with the magnetic field, a small magnet was attached right on the tumor (inset in Figure 8). The Y^{3+} concentration level of the tumors treated with the magnetic field increased greatly from 1.5 μg/g of the control group to 7.0 μg/g, implying a greatly enhanced accumulation of MFNPs to the tumor comparing with the passive tumor uptake. This efficient magnetic targeting of the MFNPs can help us use an outward magnetic field to attract those nanospheres from the circulating blood to the specific region, which would be of great importance for the further anti-tumor therapy or cellular association effects of upconversion imaging with least side effects to the normal tissue.

3.6 *In Vivo* Targeted Antitumor Efficacy of DOX Loaded MFNPs

Since the MFNPs could accumulated effectively to the specific region in response to an outward magnetic field, if we loaded some anti-tumor drugs into the MFNPs, this as-synthesized magnetic targeted "smart" drug delivery could send the drugs to, and retention at, the required body site, which would be of

great importance to magnify the cytotoxicity to the targeted tumor and reduce the side effects to the healthy tissues. Therefore, we carried out *in vivo* targeted antitumor study using the Kunming mice bearing viable H22 ascites tumors under the tumor-targeted magnetic field. Twenty-four mice bearing tumors were

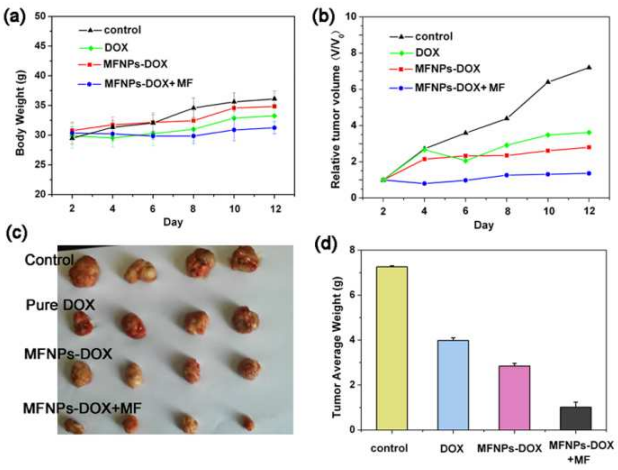

Figure 9 The body weights (a) and the relative tumor volume (b) of mice after the treatment with saline solution as control, free DOX, MFNPs-DOX and MFNPs-DOX+MR, respectively. Photographs (c) of excised tumors from euthanized representative mice (d) and mean tumor weights (d) of each group at the last day of experiment.

randomly divided into four groups (n=6) and respectively treated with saline as control, free DOX, MFNPs-DOX in the absence of the magnetic field (labeled as MFNPs-DOX) and MFNPs-DOX with the magnetic field (labeled as MFNPs-DOX+MF). Each experiment mouse was intravenously injected by the tail vein on day 1 and day 5, and the body weights and tumor sizes were measured every two days. During the experiments, no mice died. The variation trends of mean body weights and mean relative tumor volumes of each group were shown in Figure 9a, b. The weights of mice (Figure 9a) increased steadily with time and the increase trends of those four groups were similar. But the mean relative tumor volumes of each group varied differently (Figure 9b), which shows that the MFNPs-DOX+MF group showed the lowest tumor growth rate than the other there groups over a course of 12 days, demonstrating that MFNPs-DOX under tumor-targeted magnetic field is a powerful agent for *in vivo* anti-tumor therapy. The above conclusions were further verified by the photographs and average weights of the final tumors excised from mice in each group (Figure 9c, d), which showed that the group of MFNPs-DOX+MF had an average tumor growth inhibition efficacy of approximately 86%, much higher than both of the MFNPs-DOX group with an inhibition efficacy of 61% and the free DOX group with about 45%. The results were attributed to the targeted accumulation of drug-loaded MFNPs in the intratumor space as well as the sustained DOX release from MFNPs *in vivo*. The above results all indicate that the outward magnetic field targeted MFNPs could be used as a highly active magnetic targeted drug delivery.

Although the as-obtained MFNPs have an excellent therapeutic effect, the long-term bio-distribution of MFNPs is also an important issue.[47] Therefore, as given in Figure 10, the *in vivo* biodistribution of MFNPs in Kunming mice were

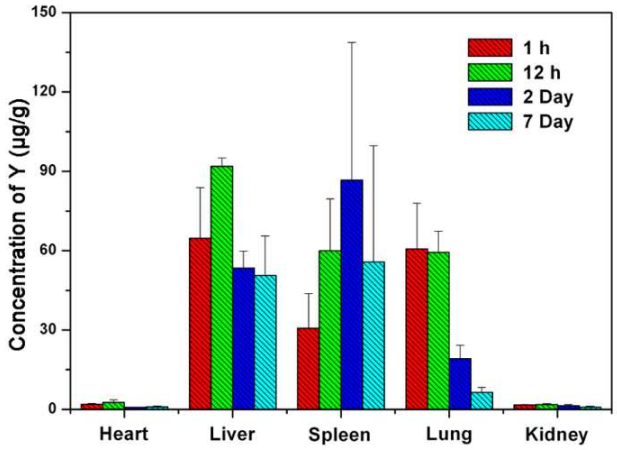

Figure 10 Biodistribution of MFNPs in mice at different time points (1 h, 12 h, 2 day, 7 day) post injection measured by ICP-AES (Fe levels).

carefully investigated by measuring Y^{3+} concentrations of various organs in order to slake the safety concern for *in vivo* therapies in the future. We can see from Figure 10 that the Y^{3+} concentrations in major organs varied with time prolonging after the tail vein injection of MFNPs. Seven days later, the concentrations of MFNPs in heart, liver, spleen, lung and kidney decreased obviously comparing with the early times, which meant that the MFNPs could be excreted gradually from the Kunming mice. It is worth to note that the Y^{3+} concentrations in spleen increased firstly as the extension of time, perhaps because the spleen is the largest organ of the immune system.[48]

4. Conclusions

In summary, an effective magnetically targeted theranostic probe $NaYF_4$:Yb, Er@mSiO_2@Fe_3O_4-PEG (MFNPs) featured with UCNPs core, mesoporous silica shell and ultrasmall Fe_3O_4 nanocrystals decoration was successfully synthesized, simultaneously achieving UCL/MR dual modal bioimaging and magnetically targeted chemo-cherapy. It is worth to note that the optimal reaction conditions were carefully conducted by changing the size of UCNPs and the amounts of Fe_3O_4 immobilized on the surface of UCNPs@mSiO_2 in order to achieve the enough bright upconversion luminescence intenisty while maintain the magnetic performance of Fe_3O_4. Both *in vitro* and *in vivo* tests show good bio-compatibility of the as-obtained MFNPs. Moreover, the *in vitro* UCL/MR bioimaging and *in vivo* magnetically targeted anti-tumor efficacy tests were carried out to prove the potential of MFNPs to be a magnetically targeted theranostic probe. Taken together, the

convenient and adjustable synthesis, good biocompatibility, low cytotoxic activity, together with the *in vitro* UCL/MR imaging and improved *in vivo* magnetically targeted anti-tumor efficiency would make our as-synthesized MFNPs useful for further theranostic applications.

Acknowledgements

This project is financially supported by the National Natural Science Foundation of China (NSFC 51332008, 51372243, 51422209), National Basic Research Program of China (2010CB327704, 2014CB643803).

Notes and references

[a] State Key Laboratory of Rare Earth Resource Utilization, Changchun Institute of Applied Chemistry, Chinese Academy of Sciences, Changchun, 130022,P. R. China. E-mail: jlin@ciac.ac.cn;cxli@ciac.ac.cn; Fax: +86-431-85698041; Tel: +86-431-85262031.

[b] University of the Chinese Academy of Sciences, Beijing 100049, P. R. China.

† Electronic Supplementary Information (ESI) available: [details of any supplementary information available should be included here]. See DOI: 10.1039/b000000x/

1 D. R. Gamelin and H. U. Güdel, Acc. Chem. Res., 2000, **33**, 235.
2 S. V. Eliseeva and J. C. G. Bünzli, Chem. Soc. Rev., 2010, **39**, 189.
3 J. Zhou, Z. Liu and F. Y. Li, Chem. Soc. Rev., 2012, **41**, 1323.
4 S. L. Gai, C. X. Li, P. P. Yang and J. Lin, Chem. Rev., 2014, **114**, 2343.
5 D. J. Gargas, E. M. Chan, A. D. Ostrowski, S. Aloni, M. V. P. Altoe, E. S. Barnard, B. Sanii, J. J. Urban, D. J. Milliron, B. E. Cohen and P. J. Schuck, Nat. Nanotech, 2014, **9**, 300.
6 Y. H. Zhang, L. X. Zhang, R. R. Deng, J. Tian, Y. Zong, D. Y. Jin and X. Liu, J. Am. Chem. Soc., 2014, **136**, 4893.
7 P. Huang, W. Zheng, S. Y. Zhou, D. T. Tu, Z. Chen, H. M. Zhu, R. F. Li, E. Ma, M. D. Huang and X. Y. Chen, Angew. Chem. Int. Ed., 2014, **53**, 1252.
8 G. Y. Chen, H. L. Qiu, P. N. Prasad and X. Y. Chen, Chem. Rev., 2014, **114**, 5161.
9 C. Y. Liu, Y. Hou and M. Y. Gao, Adv. Mater., 2014, DOI: 10.1002/adma.201305535.
10 Z. Liu, L. N. Sun, F. Y. Li, Q. Liu, L. Y. Shi, D. S. Zhang, S. Yuan, T. Liu and Y. N. Qiu, J. Mater. Chem., 2011, **21**, 17615.
11 F. Zhang, G. B. Braun, A. Pallaoro, Y. C. Zhang, Y. F. Shi, D. X. Cui, M. Moskovits, D. Y. Zhao and G. D. Stucky, Nano Lett., 2012, **12**, 61.
12 L. Cheng, K, Yang, Y. G. Li, X. Zeng, M. W. Shao, S. T. Lee and Z. Liu, Biomaterials, 2012, **33**, 2215.
13 D. M. Yang, P. A. Ma, Z. Y. Hou, Z. Y. Cheng, C. X. Li and J. Lin, Chem. Soc. Rev., 2014, DOI: 10.1039/c4cs00155a.
14 N. Niu, F. He, P. A. Ma, S. L. Gai, G. Yang, F. Qu, Y. Wang, J. Xu and P. P. Yang, ACS Appl. Mater. Interf., 2014, **6**, 3250.
15 H. Y. Xing, W. B. Bu, S. J. Zhang, X. P. Zheng, M. Li, F. Chen, Q. J. He, L. P. Zhou, W. J. Peng, Y. Q. Hua and J. L. Shi, Biomaterials, 2012, **33**, 1079.
16 Q. F. Xiao, X. P. Zheng, W. B. Bu, W. Q. Ge, S. J. Zhang, F. Chen, H. Y. Xing, Q. G. Ren, W. P. Fan, K. L. Zhao, Y. Q. Hua and J. L. Shi, J. Am. Chem. Soc., 2013, **135**, 13041.
17 X. M. Li, D. Y. Zhao and F. Zhang, Theranostics, 2013, **3**, 292.
18 H. Chen, B. Qi, T. Moore, D. C. Colvin, T. Crawford, J. C. Gore, F. Alexis, O. T. Mefford and J. N. Anker, Small, 2014, **10**, 160.
19 D. L. Ni, J. W. Zhang, W. B. Bu, H. Y. Xing, F. Han, Q. F. Xiao, Z. W. Yao, F. Chen, Q. J. He, J. N. Liu, S. J. Zhang, W. P. Fan, L. P. Zhou, W. J. Peng and J. L. Shi, ACS Nano, 2014, **8**, 1231.
20 X. F. Qiao, J. C. Zhou, J. W. Xiao, Y. F. Wang, L. D. Sun and C. H. Yan, Nanoscale, 2012, **4**, 4611.
21 D. L. Ni, W. B. Bu, S. J. Zhang, X. P. Zheng, M. Li, H. Y. Xing, Q. F. Xiao, Y. Y. Liu, Y. Q. Hua, L. P. Zhou, W. J. Peng, K. L. Zhao and J. L. Shi, Adv. Funct. Mater., 2014, DOI: 10.1002/adfm.201401609.
22 Y. Zhang, G. K. Das, V. Vijayaragavan, Q. C. Xu, P. Padmanabhan, K. K. Bhakoo, S. T. Selvan and T. T. Y. Tan, Nanoscale, 2014, DOI:10.1039/c4nr01717j.
23 C. C. Mi, J. P. Zhang, H. Y. Gao, X. L. Wu, M. Wang, Y. F. Wu, Y. Q. Di, Z. Q. Xu, C. B. Mao and S. K. Xu, Nanoscale, 2010, **2**, 1141.
24 L. Zhang, Y. S Wang, Y Yang, F Zhang, W. F. Dong, S. Y. Zhou, W. H. Pei, H. D. Chen and H. B. Sun. Chem. Commun., 2012, **48**, 11238.
25 N. A. Frey, S. Peng, K. Cheng and S. H. Sun, Chem. Soc. Rev., 2009, **38**, 2532.
26 J. Liu, S. Z. Qiao, Q. H. Hu and G. Q. (Max) Lu, Small, 2011, **7**, 425.
27 P. P. Yang, S. L. Gai and J. Lin, Chem. Soc. Rev., 2012, **41**, 3679.
28 D. Singh, J. M. McMillan, X. M. Liu, H. M .Vishwasrao, A. V. Kabanov, M. Sokolsky-Papkov and H. E Gendelman, Nanomedicine, 2014, **9**, 469.
29 M. Vallet-Regí, A. Rámila, R. P. del Real and J. Pérez-Pariente, Chem. Mater., 2001, **13**, 308.
30 J. E. Lee, N. Lee, T. Kim, J. Kim and T. Hyeon, Acc. Chem. Res., 2011, **44**, 893.
31 C. Argyo, V. Weiss, C. Bräuchle and T. Bein, Chem. Mater., 2014, **26**, 435-451.
32 D. Hu, M. Chen, Y. Gao, F. Li and L. Wu, J. Mater. Chem., 2011, **21**, 11276.
33 S. L. Gai, P. P. Yang, C. X. Li, W. X. Wang, Y. L. Dai, N. Niu and J. Lin, Adv. Funct. Mater., 2010, **20**, 1166.
34 X. J. Zhu, J. Zhou, M. Chen, M. Shi, W. Feng and F. Y. Li, Biomaterials, 2012, **33**, 4618.
35 Z. Q. Li, Y. Zhang and S. Jiang, Adv. Mater., 2008, **20**, 4765.
36 S. Sun, H. Zeng, D. B. Robinson, S. Raoux, P. M. Rice, S. X. Wang and G. Li, J. Am. Chem. Soc., 2004, **126**, 273.
37 W. F. Ma, K. Y. Wu, J. Tang, D. Li, C. Wei, J. Guo, S. L. Wang and C. C. Wang, J. Mater. Chem., 2012, **22**, 15206.
38 J. E. Lee, N. Lee, H. Kim, J. Kim, S.H. Choi, J. H. Kim, T. Kim, I. C. Song, S. P. Park, W. K. Moon and T. Hyeon, J. Am. Chem. Soc., 2009, **132**, 552.
39 C. X. Li, Z. Y. Hou, Y. L. Dai, D. M. Yang, Z. Y. Cheng, P. A. Ma and J. Lin, Biomaterials, 2013, **1**, 213.
40 L. D. Sun, Y. F. Wang and C. H. Yan, Acc. Chem. Res., 2014, **47**, 1001.
41 J. Shan and Y. Ju, Nnaotechnology, 2009, **20**, 275603.

42 Y. Y. Chen, P. A. Ma, D. M. Yang, Y. Wu, Y. L. Dai, C. X. Li and J. Lin, Chem. Asian J., 2014, **9**, 506.
43 J. Shen, L. D. Sun, Y. W. Zhang and C. H. Yan, Chem. Commun., 2010, **46**, 5731.
44 J. N. Liu, J. W. Bu, W. B. Bu, S. J. Zhang, L. M. Pan, W. P. Fan, F. Chen, L. P. Zhou, W. J. Peng, K. L. Zhao, J. L. Du and J. L. Shi, Angew. Chem. Int. Ed., 2014, **53**, 4551.
45 W. Wei, G. H. Ma, G. Hu, D. Yu, T. Mcleish, Z. G. Su and Z. Y. Shen, J. Am. Chem. Soc., 2008, **130**, 15808.
46 Y. I. Park, K. T. Lee, Y. D. Suh and T. Hyeon, Chem. Soc. Rev., 2014, DOI: 10.1039/c4cs00173g.
47 Z. Y. Cheng, Y. L. Dai, X. J. Kang, C. X. Li, S. S. Huang, H. Z. Lian, Z. Y. Hou, P. A. Ma and J. Lin, Biomaterials, 2014, **35**, 6359.
48 Y. L. Dai, H. H. Xiao, J. H. Liu, Q. H. Yuan, P. A. Ma, D. M. Yang, C. X. Li, Z. Y. Cheng, Z. Y. Hou, P. P. Yang and J. Lin, J. Am. Chem. Soc., 2013, **135**, 18920.

TOC

In this work, we show a convenient and adjustable synthesis of multifunctional nanoparticles $NaYF_4$:Yb, Er@mSiO_2@Fe_3O_4-PEG (MFNPs) that can simultaneously combine upconversion luminescence (UCL) imaging, magnetic resonance (MR) imaging and magnetically targeted drug delivery in one platform. The integration of UCNPs, mesoporous silica and Fe_3O_4 nanocrystals that can combine the diagnostic/therapeutic functions within a single platform, may provide a more advanced way for the accurate diagnosis and magnetically targeted therapy of cancer.